Electronic Research Archive

http://www.aimspress.com/journal/era

ERA, 30(2): 492–514.
DOI: 10.3934/era.2022026
Received: 12 October 2021
Revised: 14 November 2021
Accepted: 16 November 2021
Published: 10 February 2022

Research article

A harmonic function method for EEG source reconstruction

Hongguang Xi and Jianzhong Su*

Department of Mathematics, The University of Texas at Arlington, Arlington, TX 76019, USA

* **Correspondence:** Email: su@uta.edu.

Abstract: In this paper we study a harmonic function method for dipolar source reconstruction, and implemented the numerical simulations. We propose a new error estimate and provide a rigorous proof of the estimate. Then, we validate our method in computer-simulated data and study its numerical stability in different noise levels. It is shown that the harmonic function method can be used to quickly and accurately locate the active regions in EEG source reconstruction.

Keywords: harmonic analysis; inverse problem; error bounds

1. Introduction

Neuronal activities generate the electrical current in the brain, and further result in the potential changes over the scalp. Electroencephalography (EEG) is a technique used to record the potential changes on the scalp. Even though fMRI, PET, MEG and other brain-imaging tools are widely used in brain research, they are limited by low spatial/temporal resolution, cost, mobility and suitability for long-term monitoring. For example, fMRI has the advantage of providing spatially-resolved data, but suffers from an ill-posed temporal inverse problem, i.e., a map with regional activations does not contain information about when and in which order these activations have occurred [1]. In contrast, EEG signals have been successfully used to obtain useful diagnostic information (neural oscillations and response times) in clinical contexts. Further, they present the advantage to be highly portable, inexpensive, and can be acquired at the bedside or in real-life environments with a high temporal resolution. Because of the lack of significant patient risks, EEG is additionally suited for long-term monitoring.

EEG offers the possibility of measuring the electrical activity of neuronal cell assemblies on the sub-millisecond time scale [2–4]. EEG source imaging further identifies the positions or distributions of electric fields based on EEG signals collected on the scalp [5]. This new tool is widely used in cognitive neuroscience research, and has also found important applications in clinical neuroscience such as neurology, psychiatry and psychopharmacology [6, 7]. In cognitive neuroscience, the majority

of the studies investigate the temporal aspects of information processing by analyzing event related potentials (ERP). In neurology, the study of sensory or motor evoked potentials is of increasing interest, but the main clinical application concerns with the localization of epileptic foci. In psychiatry and psychopharmacology, a major focus of interest is the localization of sources of certain EEG frequency bands. Localizing the activity sources of a given scalp EEG measurement is achieved by solving the so-called inverse problem [8]. These kinds of inverse problems are usually ill-posed and their solutions are non-unique [9, 10].

Leahy *et al.* [11] investigated the accuracy of forward and inverse techniques for EEG and MEG dipole localization using a human skull phantom. El Badia and Ha-Duong [12] established an algebraic method to identify the number, locations and moments of electrostatic dipoles in 2D or 3D domain from the Cauchy data on the boundary. Chafik *et al.* [13] further provided an error estimate without proof. Nara and Ando [14] provided a new projective method for 3D source reconstruction by projecting the sources onto a Riemann sphere. Kang and Lee [15] proposed an algorithm for solving the inverse source problem of a meromorphic function and apply their method to an electrical impedance tomography (EIT) problem. El Badia [16] established a uniqueness result and a local Lipschitz stability estimate for an anisotropic elliptic equation, assuming that the sources are a linear combination of a finite number of monopoles and dipoles. The author also proposed a global Lipschitz stability estimate for dipolar sources. Baratchart *et al.* [17] solved the inverse source problem by locating the singularities of a meromorphic function from the 2D boundary measurements using best rational or meromorphic approximations.

Chung and Chung [18] proposed an algorithm for detecting the combination of monopolar and multipolar point sources for elliptic equations in the 2D domain from the Neumann and Dirichlet boundary data. Kandasmamy *et al.* [19] proposed a novel technique, called "analytic sensing", to estimate the positions and intensities of point sources in 2D for a Poisson's equation. Analytic sensing also used the reciprocity gap principle, but with a novel design of an analytic function which behaved like a sensor. The authors evaluated their estimation accuracy by Cramér-Rao lower bound. Nara and Ando [20] proposed an algebraic method to localize the positions of multiple poles in meromorphic function field from an incomplete boundary. They investigated the accuracy of the algorithm for the open arc or the closed arc, and for the arc enclosing the poles or not enclosing the poles. El Badia and Nara [21] established the uniqueness and local stability result for the inverse source problem of the Helmholtz equation in an interior domain, assuming the source is composed of multiple point sources.

Clerc *et al.* [22] applied best rational approximation techniques in the complex plane to EEG source localization and offered stability estimates. Mdimagh and Ben Saad [23] identified the point sources in a scalar problem modeled by Helmholtz equation, using reciprocity gap principle and assuming the sources are harmonic in time. They proved local Lipschitz stability by two methods: one was derived from the Gâteaux differentiability, and the other used particular test functions in the reciprocity gap functional. Vorwerk *et al.* [24] studies the important role of head tissue conductivity in EEG dipole reconstruction. Rubega *et al.* [25] estimated EEG source dipole orientation based on singular-value decomposition. Michel and Brunet provided a thorough review on EEG source imaging. There exist several reconstruction methods, such as minimum norm estimates (MNE) [26], low resolution electrical tomography (LORETA) [27,28] or multiple-signal classification algorithm (MUSIC) [29,30], etc.

Recently, Muñoz-Gutiérrez *et al.* [31] managed to improve the accuracy of EEG source reconstruc-

tion by decomposing the EEG signals into frequency bands with different methods, such as empirical mode decomposition (EMD) and wavelet transform (WT). Kaur *et al.* [32] presented a new method of EEG source localization using variational mode decomposition (VMD) and standardized the low resolution brain electromagnetic tomography (sLORETA) inverse model. Their VMD-sLORETA model could locate EEG sources in the brain in a very accurate way. Oikonomou and Kompatsiaris [33] developed a novel Bayesian approach for EEG source localization. They incorporated a new sparse prior for the localization of EEG sources with the variational Bayesian (VB) framework and obtained more accurate localization of EEG sources than state-of-the-art approaches.

In our study we need new methods to detect small changes in EEG source for which dipole methods have advantage. We followed the analytic dipole method by El Badia and Ha-Duong [12] and derived a new error estimate for this source localization method. We provided a mathematical proof of this estimate. We then use simulated data to validate the method. The simulation results support our error estimation, which has a different distance power than a similar error estimate in [22].

We organize the rest of the paper as follows. In section 2, we introduce the method and its formulation. In section 3, we provide the error estimate of an inverse EEG source localization problem in a bounded domain and its mathematical proof. In section 4, we use simulated data to valid the method and error estimate. A brief conclusion and discussion is in Section 5.

2. Mathematical model of EEG problem

2.1. Mathematical model

The electric field $\mathbf{E}$ is the negative gradient of the potential u.

$$\mathbf{E} = -\nabla u. \tag{2.1}$$

The quasi-static approximation means all time derivatives in the equation are set to zero. By quasi-static approximation of Maxwell equation $\nabla \times \mathbf{H} - \dfrac{\partial \mathbf{D}}{\partial t} = \mathbf{J}$, we have

$$\nabla \times \mathbf{H} = \mathbf{J}$$

where $\mathbf{H}$ is the magnetizing field, $\mathbf{J}$ is the total current density, and $\mathbf{D}$ is the displacement field.

Since the divergence of a curl is always zero, we have

$$\nabla \cdot (\nabla \times \mathbf{H}) = \nabla \cdot \mathbf{J} = 0.$$

EEG problem can be modeled by a Poisson equation.

$$\begin{aligned} -\nabla \cdot (\sigma \nabla u) &= \nabla \cdot (\sigma \mathbf{E}) \\ &= \nabla \cdot (\mathbf{J} - \mathbf{J}^p) \\ &= \underbrace{\nabla \cdot \mathbf{J}}_{=0} - \nabla \cdot \mathbf{J}^p \\ &= -\nabla \cdot \mathbf{J}^p \\ &= F, \end{aligned}$$

where σ is the conductivity, $\mathbf{J}^p$ is the primary current density, and F is the source term.

2.2. Source model

If we assume the source is composed of a finite number of point charges, then by linear combination, we have

$$F = \sum_{k=1}^{m} q_k \delta(\mathbf{r} - \mathbf{r}_k), \tag{2.2}$$

where m is the number of point charges, q_k are values of charges, and $\mathbf{r}_k$ are the locations of the point charges.

If we assume the source is composed of a finite number of dipoles, we have

$$F = -\sum_{k=1}^{m} \mathbf{p}_k \cdot \nabla \delta(\mathbf{r} - \mathbf{r}_k),$$

where m is the number of dipoles, $\mathbf{p}_k$ are the moments (or strengths) of the dipoles, and $\mathbf{r}_k$ are the centers of dipoles.

2.3. The harmonic function method of identifying dipolar sources

The dipolar source reconstruction problem can be viewed as a Poisson problem.

$$\Delta u = \sum_{k=1}^{m} \mathbf{p}_k \cdot \nabla \delta(\mathbf{r} - \mathbf{r}_k) \text{ in } \Omega, \tag{2.3}$$

$$u = f \text{ on } \Gamma, \tag{2.4}$$

$$\frac{\partial u}{\partial \nu} = \varphi \text{ on } \Gamma, \tag{2.5}$$

where f and φ are known, and ν is the outer unit normal vector.

We will use the concept of reciprocity gap functional [34]:

$$\begin{aligned} R(v) &= \left\langle \frac{\partial u}{\partial \nu}, v \right\rangle_{H^{1/2}(\Gamma), H^{-1/2}(\Gamma)} - \left\langle u, \frac{\partial v}{\partial \nu} \right\rangle_{H^{1/2}(\Gamma), H^{-1/2}(\Gamma)} \\ &= \langle \varphi, v \rangle_{H^{1/2}(\Gamma), H^{-1/2}(\Gamma)} - \left\langle f, \frac{\partial v}{\partial \nu} \right\rangle_{H^{1/2}(\Gamma), H^{-1/2}(\Gamma)}, \end{aligned} \tag{2.6}$$

where v is a harmonic function in Ω:

$$v \in H(\Omega) = \{w \in H^1(\Omega) \mid \Delta w = 0\}. \tag{2.7}$$

By Green's formula, we have

$$R(v) = -\sum_{k=1}^{m} \mathbf{p}_k \cdot \nabla v(\mathbf{r} - \mathbf{r}_k), \forall v \in H(\Omega). \tag{2.8}$$

Let m be the number of dipoles in the brain. Assume $m \leq M$ in our problem, i.e., there is an upper bound for the number of dipoles.

Let us consider the harmonic polynomials

$$v_j(x,y) = (x+iy)^j, \quad j \in \mathbb{N}.$$

Then, in 2D case

$$\begin{aligned}
R(v_j) &= -\sum_{k=1}^{m} \mathbf{p}_k \cdot \nabla v_j(\mathbf{r}_k) \\
&= -\sum_{k=1}^{m} \begin{bmatrix} p_{k1} \\ p_{k2} \end{bmatrix} \cdot \nabla (x_k + iy_k)^j \\
&= -\sum_{k=1}^{m} \begin{bmatrix} p_{k1} \\ p_{k2} \end{bmatrix} \cdot \left[\begin{matrix} \frac{\partial}{\partial x}(x+iy)^j \\ \frac{\partial}{\partial y}(x+iy)^j \end{matrix} \right]_{x=x_k, y=y_k} \\
&= -\sum_{k=1}^{m} \begin{bmatrix} p_{k1} \\ p_{k2} \end{bmatrix} \cdot \begin{bmatrix} j(x_k+iy_k)^{j-1} \cdot 1 \\ j(x_k+iy_k)^{j-1} \cdot i \end{bmatrix} \\
&= -\sum_{k=1}^{m} \begin{bmatrix} p_{k1} \\ p_{k2} \end{bmatrix} \cdot \begin{bmatrix} 1 \\ i \end{bmatrix} j(x_k+iy_k)^{j-1} \\
&= -j \sum_{k=1}^{m} (p_{k1} + ip_{k2})(x_k+iy_k)^{j-1}.
\end{aligned}$$

We define

$$\beta_j := \frac{R(v_j)}{-j} = \sum_{k=1}^{M} (p_{k1} + ip_{k2})(x_k+iy_k)^{j-1}, \quad j = 1, 2, ..., 2M-1. \tag{2.9}$$

Let

$$\eta_j = \begin{bmatrix} \beta_j \\ \beta_{j+1} \\ \vdots \\ \beta_{j+M-1} \end{bmatrix} \in \mathbb{C}^M, \quad 1 \le j \le M, \tag{2.10}$$

and

$$Z_i = \left[\eta_i, \eta_{i+1}, ..., \eta_{i+M-1}\right] = \begin{bmatrix} \beta_i & \beta_{i+1} & \cdots & \beta_{i+M-1} \\ \beta_{i+1} & \beta_{i+2} & \cdots & \beta_{i+M} \\ \vdots & & & \\ \beta_{i+M-1} & \beta_{i+M} & \cdots & \beta_{i+2M-2} \end{bmatrix}, \quad i \in \mathbb{N}.$$

Then,

$$Z_1 = \left[\eta_1, \eta_2, ..., \eta_M\right] = \begin{bmatrix} \beta_1 & \beta_2 & \cdots & \beta_M \\ \beta_2 & \beta_3 & \cdots & \beta_{M+1} \\ \vdots & & & \\ \beta_M & \beta_{M+1} & \cdots & \beta_{2M-1} \end{bmatrix}.$$

The number m of dipoles is estimated as the rank of Z_1.

Now we can reduce the size of the matrix by recalculating β_j and η_j with M replaced by m. Then, the m vectors $\eta_1, ..., \eta_m$ are independent.

To get the estimates of the positions we need to construct an $m \times m$ matrix T such that $\eta_{j+1} = T\eta_j$, $j = 1, ..., m$. Then,

$$[\eta_2, ..., \eta_{m+1}] = T[\eta_1, ..., \eta_m].$$

So,

$$\begin{aligned} T &= [\eta_2, ..., \eta_{m+1}][\eta_1, ..., \eta_m]^{-1} \\ &= \begin{bmatrix} \beta_2 & \beta_3 & \cdots & \beta_{m+1} \\ \beta_3 & \beta_4 & \cdots & \beta_{m+2} \\ \vdots & & & \\ \beta_{m+1} & \beta_{m+2} & \cdots & \beta_{2m} \end{bmatrix} \begin{bmatrix} \beta_1 & \beta_2 & \cdots & \beta_m \\ \beta_2 & \beta_3 & \cdots & \beta_{m+1} \\ \vdots & & & \\ \beta_m & \beta_{m+1} & \cdots & \beta_{2m-1} \end{bmatrix}^{-1} \\ &= Z_2 Z_1^{-1}. \end{aligned}$$

The positions of dipoles are estimated as the eigenvalues of T.

We now show that the eigenvalues of T are the positions of dipoles. Let us first look at an example $\eta_2 = T\eta_1$.

$$\begin{aligned} T\eta_1 &= T \begin{bmatrix} \beta_1 \\ \beta_2 \\ \vdots \\ \beta_m \end{bmatrix} = T \begin{bmatrix} p_1 + p_2 + \cdots + p_m \\ p_1 S_1 + p_2 S_2 + \cdots + p_m S_m \\ \vdots \\ p_1 S_1^{m-1} + p_2 S_2^{m-1} + \cdots + p_m S_m^{m-1} \end{bmatrix} \\ &= p_1 T \begin{bmatrix} 1 \\ S_1 \\ \vdots \\ S_1^{m-1} \end{bmatrix} + p_2 T \begin{bmatrix} 1 \\ S_2 \\ \vdots \\ S_2^{m-1} \end{bmatrix} + \cdots + p_m T \begin{bmatrix} 1 \\ S_m \\ \vdots \\ S_m^{m-1} \end{bmatrix}, \end{aligned}$$

where $p_k = p_{k1} + ip_{k2}, k = 1, 2, ..., m$ is the moment and $S_k = x_k + iy_k, k = 1, 2, ..., m$ is the position.

$$\begin{aligned} \eta_2 &= \begin{bmatrix} \beta_2 \\ \beta_3 \\ \vdots \\ \beta_{m+1} \end{bmatrix} = \begin{bmatrix} p_1 S_1 + p_2 S_2 + \cdots + p_m S_m \\ p_1 S_1^2 + p_2 S_2^2 + \cdots + p_m S_m^2 \\ \vdots \\ p_1 S_1^m + p_2 S_2^m + \cdots + p_m S_m^m \end{bmatrix} \\ &= p_1 S_1 \begin{bmatrix} 1 \\ S_1 \\ \vdots \\ S_1^{m-1} \end{bmatrix} + p_2 S_2 \begin{bmatrix} 1 \\ S_2 \\ \vdots \\ S_2^{m-1} \end{bmatrix} + \cdots + p_m S_m \begin{bmatrix} 1 \\ S_m \\ \vdots \\ S_m^{m-1} \end{bmatrix}, \end{aligned}$$

where $p_k = p_{k1} + ip_{k2}, k = 1, 2, ..., m$ is the moment and $S_k = x_k + iy_k, k = 1, 2, ..., m$ is the position.

Since $\begin{bmatrix} 1 \\ S_1 \\ \vdots \\ S_1^{m-1} \end{bmatrix}, \begin{bmatrix} 1 \\ S_2 \\ \vdots \\ S_2^{m-1} \end{bmatrix}, ..., \begin{bmatrix} 1 \\ S_m \\ \vdots \\ S_m^{m-1} \end{bmatrix}$ are independent and the results are similar for $\eta_{j+1} = T\eta_j$, $j = 1, 2, ..., m$, we know $S_1, S_2, ..., S_m$ are just the eigenvalues of T.

Now the question is how to get T. Only η_1 and η_2 are not enough to determine T because vectors have no inverse. So, we use the redundant information to construct the matrices Z_1 and Z_2 such that $T = Z_2 Z_1^{-1}$, where Z_1 is invertible because $\eta_1, ..., \eta_m$ are independent.

To estimate the moments of dipoles we will write Eq (2.9) in matrix form. Notice that now we use m instead of M.

$$\begin{bmatrix} \beta_1 \\ \beta_2 \\ \vdots \\ \beta_m \end{bmatrix} = \begin{bmatrix} S_1^0 & S_2^0 & \cdots & S_m^0 \\ S_1^1 & S_2^1 & \cdots & S_m^1 \\ \vdots & & & \\ S_1^{m-1} & S_2^{m-1} & \cdots & S_m^{m-1} \end{bmatrix} \begin{bmatrix} p_1 \\ p_2 \\ \vdots \\ p_m \end{bmatrix}, \tag{2.11}$$

where $p_k = p_{k1} + ip_{k2}, k = 1, 2, ..., m$ is the moment and $S_k = x_k + iy_k, k = 1, 2, ..., m$ is the position.

We can write Eq (2.11) in matrix form

$$\mathbf{b} = \mathbf{S}\mathbf{p}, \tag{2.12}$$

where $\mathbf{b} = \begin{bmatrix} \beta_1 \\ \beta_2 \\ \vdots \\ \beta_m \end{bmatrix}, \mathbf{S} = \begin{bmatrix} S_1^0 & S_2^0 & \cdots & S_m^0 \\ S_1^1 & S_2^1 & \cdots & S_m^1 \\ \vdots & & & \\ S_1^{m-1} & S_2^{m-1} & \cdots & S_m^{m-1} \end{bmatrix}$, and $\mathbf{p} = \begin{bmatrix} p_1 \\ p_2 \\ \vdots \\ p_m \end{bmatrix}$. Then, the moments of dipoles in 2D are estimated as

$$\mathbf{p} = \mathbf{S}^{-1}\mathbf{b}. \tag{2.13}$$

2.4. Optimization of linear operator

Equation (2.13) works in the ideal case of no noise. In reality, due to the noise in the measurements and in the sources, we need find a linear operator $\mathbf{L}$ to estimate the moments, i.e.,

$$\tilde{\mathbf{p}} = \mathbf{L}\mathbf{b} \tag{2.14}$$

where $\tilde{\mathbf{p}}$ represents the estimates of the moments, and $\mathbf{b}$ represents the quantities obtained from the measurements.

Considering the noise accompanied in the measurements, we rewrite Eq (2.12) as

$$\mathbf{b} = \mathbf{S}\mathbf{p} + \mathbf{n},$$

where $\mathbf{n}$ is a random vector of mean 0. Let $\mathbf{N}$ be the covariance matrix of $\mathbf{n}$. Also, assume that $\tilde{\mathbf{p}}$ is normally distributed with mean $\mathbf{p}$ and its covariance matrix is $\mathbf{P}$.

Using multiple measurements and the statistical estimation theory we can find the linear operator $\mathbf{L}$ which minimizes the expected difference $Err_{\mathbf{L}}$ between the estimated moments $\tilde{\mathbf{p}}$ and the exact moments $\mathbf{p}$.

$$\begin{aligned} Err_{\mathbf{L}} &= \langle ||\tilde{\mathbf{p}} - \mathbf{p}||^2 \rangle \\ &= \langle ||\mathbf{L}\mathbf{b} - \mathbf{p}||^2 \rangle \\ &= \langle ||\mathbf{L}(\mathbf{S}\mathbf{p} + \mathbf{n}) - \mathbf{p}||^2 \rangle \\ &= \langle ||(\mathbf{L}\mathbf{S} - \mathbf{I})\mathbf{p} + \mathbf{L}\mathbf{n}||^2 \rangle \\ &= \langle ||\mathbf{M}\mathbf{p} + \mathbf{L}\mathbf{n}||^2 \rangle \quad (\text{where } \mathbf{M} = \mathbf{L}\mathbf{S} - \mathbf{I}) \end{aligned}$$

$$
\begin{aligned}
&= \langle \|\mathbf{Mp}\|^2 \rangle + \langle \|\mathbf{Ln}\|^2 \rangle \quad \text{(by independence of } \mathbf{p} \text{ and } \mathbf{n}) \\
&= Tr(\mathbf{MPM}^T) + Tr(\mathbf{LNL}^T).
\end{aligned}
$$

Setting the gradient of $Err_{\mathbf{L}}$ to 0 and solving for $\mathbf{L}$, we get the optimal linear operator

$$\mathbf{L} = \mathbf{PS}^T(\mathbf{SPS}^T + \mathbf{N})^{-1}. \tag{2.15}$$

Then, by Eq (2.14) we get the best estimates of the moments.

2.5. Uniqueness of solutions

Theorem 2.1 (Uniqueness of solutions)**.** *Let $u_i, i = 1, 2$ be the solutions of the problems*

$$-\nabla \cdot (\sigma \nabla u_i) = \sum_{k=1}^{m_i} \mathbf{p}_k^{(i)} \cdot \nabla \delta_{S_k^{(i)}} \text{ in } \Omega,$$

$$\frac{\partial u_i}{\partial \nu} = \varphi \text{ on } \Gamma,$$

such that

$$u_1 = u_2 \text{ on } \Gamma,$$

then

$$\begin{aligned}
m_1 &= m_2 = m, \\
\mathbf{p}_k^{(1)} &= \mathbf{p}_k^{(2)}, \forall k = 1, 2, ..., m, \\
S_k^{(1)} &= S_k^{(2)}, \forall k = 1, 2, ..., m.
\end{aligned}$$

The solution of Poisson equation is the convolution of the fundamental solution of Laplace equation and the source function.

$$w(x) = \frac{1}{2\pi} \left[\sum_{k=1}^{m_2} \frac{\mathbf{p}_k \cdot (x - S_k)}{\left| x - S_k^{(2)} \right|^2} - \sum_{k=1}^{m_1} \frac{\mathbf{p}_k \cdot (x - S_k)}{\left| x - S_k^{(1)} \right|^2} \right], n = 2.$$

$$w(x) = \frac{-1}{4\pi} \left[\sum_{k=1}^{m_2} \frac{\mathbf{p}_k \cdot (x - S_k)}{\left| x - S_k^{(2)} \right|^3} - \sum_{k=1}^{m_1} \frac{\mathbf{p}_k \cdot (x - S_k)}{\left| x - S_k^{(1)} \right|^3} \right], n = 3.$$

3. Error estimates of positions

As EEG imaging data are typically noisy, especially determining the rank of a near singular matrix is very unstable, the error of the numerical reconstruction method needs to be studied. Chafik *et al.* [12, 13] proposed that when the norms of the perturbations ($g = \tilde{f} - f, h = \tilde{\varphi} - \varphi$) are small in $H^{1/2} \times H^{-1/2}$, there exist $a > 0$ and $b > 0$ such that $\forall k = 1, 2, ..., m$,

$$\begin{aligned}
\|\tilde{S}_k - S_k\|_2 \quad \leq \quad & \frac{m(1 - R^m)}{d^{m-1}(1 - R)} \max \left\{ \binom{m-1}{j} R^j, 0 \leq j \leq m - 1 \right\} \cdot \\
& \cdot \left(a \|g\|_{H^{1/2}(\Gamma)} + b \|h\|_{H^{-1/2}(\Gamma)} \right),
\end{aligned} \tag{3.1}$$

where $S_k = x_k + iy_k$ is the exact position of the kth dipole, $\tilde{S}_k = \tilde{x}_k + i\tilde{y}_k$ is the estimated position of the kth dipole, d is the minimal distance between S_k and $\tilde{S}_k$, and $R \neq 1$ is a real number bigger than the norm of any point on Γ. However, the analysis is not given by Chafik *et al*.

Here we present a new error estimate and provide a proof.

Theorem 3.1. *Suppose m dipoles are enclosed in a circular boundary of radius R. The potential f on the boundary and the gradient of the potential φ perpendicular to the boundary are known. If T is the measurements without noise, and $\tilde{T}$ is the measurements with noise, then the error estimate is given by*

$$\begin{aligned} & \|T - \tilde{T}\|_\infty \\ \leq\ & 2m\left(\|\varphi\|_2 R^{2m}\sqrt{2\pi R} + \|f\|_2 R^{2m}\sqrt{2\pi R}\right)\left(\frac{m!m^{m-1}p_{max}^{m-1}R^{m(m-1)}}{p_{min}^m d^{m(m-1)}}\right) \\ & +2m^2\left(\|\varphi\|_2 R^{2m}\sqrt{2\pi R} + \|f\|_2 R^{2m}\sqrt{2\pi R}\right)^2\left(\frac{m!m^{m-1}p_{max}^{m-1}R^{m(m-1)}}{p_{min}^m d^{m(m-1)}}\right)^2, \end{aligned} \tag{3.2}$$

where p is the moment of dipoles and d is the smallest distance between any two dipoles.

Proof. We define

$$Z_i = \begin{bmatrix} \beta_i & \beta_{i+1} & \cdots & \beta_{i+m-1} \\ \beta_{i+1} & \beta_{i+2} & \cdots & \beta_{i+m} \\ \vdots & & & \\ \beta_{i+m-1} & \beta_{i+m} & \cdots & \beta_{i+2m-2} \end{bmatrix}, \quad i \in \mathbb{N}.$$

Then,

$$Z_1 = \begin{bmatrix} \beta_1 & \beta_2 & \cdots & \beta_m \\ \beta_2 & \beta_3 & \cdots & \beta_{m+1} \\ \vdots & & & \\ \beta_m & \beta_{m+1} & \cdots & \beta_{2m-1} \end{bmatrix}.$$

where

$$\beta_j = \sum_{k=1}^{m} p_k S_k^{j-1} = \sum_{k=1}^{m}(p_{k1} + ip_{k2})(x_k + iy_k)^{j-1}, \quad j = 1, 2, ..., 2m-1.$$

$$\begin{aligned} \det(Z_1) &= \begin{vmatrix} \beta_1 & \beta_2 & \cdots & \beta_m \\ \beta_2 & \beta_3 & \cdots & \beta_{m+1} \\ \vdots & & & \\ \beta_m & \beta_{m+1} & \cdots & \beta_{2m-1} \end{vmatrix} \\ &= \begin{vmatrix} \sum p_k & \sum p_k S_k & \cdots & \sum p_k S_k^{m-1} \\ \sum p_k S_k & \sum p_k S_k^2 & \cdots & \sum p_k S_k^m \\ \vdots & & & \\ \sum p_k S_k^{m-1} & \sum p_k S_k^m & \cdots & \sum p_k S_k^{2m-2} \end{vmatrix} \\ &= \sum_{m_1 \neq m_2 \neq \cdots \neq m_m} \tau(m_1, m_2, ..., m_m) \cdot p_{m_1} p_{m_2} \cdots p_{m_m} \begin{vmatrix} 1 & S_{m_2} & \cdots & S_{m_m}^{m-1} \\ S_{m_1} & S_{m_2}^2 & \cdots & S_{m_m}^m \\ \vdots & & & \\ S_{m_1}^{m-1} & S_{m_2}^m & \cdots & S_{m_m}^{2m-2} \end{vmatrix} \end{aligned}$$

$$
\begin{aligned}
&= \sum_{m_1\neq m_2\neq\cdots\neq m_m} \tau(m_1,m_2,...,m_m)\cdot p_{m_1}p_{m_2}\cdots p_{m_m}\begin{vmatrix} 1 & 1 & \cdots & 1 \\ S_{m_1} & S_{m_2} & \cdots & S_{m_m} \\ \vdots & & & \\ S_{m_1}^{m-1} & S_{m_2}^{m-1} & \cdots & S_{m_m}^{m-1} \end{vmatrix}\cdot \\
&\quad \cdot S_{m_1}^0 S_{m_2}^1\cdots S_{m_m}^{m-1} \\
&= p_1p_2\cdots p_m\begin{vmatrix} 1 & 1 & \cdots & 1 \\ S_{m_1} & S_{m_2} & \cdots & S_{m_m} \\ \vdots & & & \\ S_{m_1}^{m-1} & S_{m_2}^{m-1} & \cdots & S_{m_m}^{m-1} \end{vmatrix}\cdot \\
&\quad \cdot\left(\sum_{m_1\neq m_2\neq\cdots\neq m_m} \tau(m_1,m_2,...,m_m)\cdot S_{m_1}^0 S_{m_2}^1\cdots S_{m_m}^{m-1}\right) \\
&= p_1p_2\cdots p_m\begin{vmatrix} 1 & 1 & \cdots & 1 \\ S_{m_1} & S_{m_2} & \cdots & S_{m_m} \\ \vdots & & & \\ S_{m_1}^{m-1} & S_{m_2}^{m-1} & \cdots & S_{m_m}^{m-1} \end{vmatrix}\cdot\begin{vmatrix} 1 & 1 & \cdots & 1 \\ S_{m_1} & S_{m_2} & \cdots & S_{m_m} \\ \vdots & & & \\ S_{m_1}^{m-1} & S_{m_2}^{m-1} & \cdots & S_{m_m}^{m-1} \end{vmatrix} \\
&= p_1p_2\cdots p_m\prod_{1\le i<j\le m}(S_i-S_j)^2.
\end{aligned}
$$

Here, $(m_1, m_2, ..., m_m)$ is any permutation of $(1, 2, ..., m)$ and $\tau(m_1, m_2, ..., m_m)$ is the sign determined by the permutation.

The maximum absolute row sum norm is defined by

$$\|A\|_\infty = \max_i \sum_j |a_{ij}|,$$

where A is a matrix. When A is a vector, $\|A\|_\infty = \max_i |a_i|$.

In the following proof we will use an important inequality:

$$\|a(x)b(x) - a(y)b(y)\|_\infty \le \|a(x) - a(y)\|_\infty \cdot \|b(x)\|_\infty + \|b(x) - b(y)\|_\infty \cdot \|a(x)\|_\infty$$

where $a(x)$ and $b(x)$ can be scalar, vector, or matrix.

By Cauchy-Schwarz inequality, we have

$$
\begin{aligned}
&R(v_j) \\
&= \left\langle \varphi, v_j\right\rangle - \left\langle f, \frac{\partial v_j}{\partial \nu}\right\rangle \\
&= \int_\Gamma \varphi\cdot v_j ds - \int_\Gamma f\cdot\frac{\partial v_j}{\partial\nu}ds \\
&= \int_\Gamma \varphi\cdot(x+iy)^j ds - \int_\Gamma f\cdot\frac{\partial(x+iy)^j}{\partial\nu}ds
\end{aligned}
$$

$$\begin{aligned}
&\leq \left(\int_\Gamma \varphi^2 ds\right)^{1/2}\left(\int_\Gamma (x+iy)^{2j} ds\right)^{1/2} + \left(\int_\Gamma f^2 ds\right)^{1/2}\left(\int_\Gamma \left(\frac{\partial (x+iy)^j}{\partial \nu}\right)^2 ds\right)^{1/2}\\
&\leq \left(\int_\Gamma \varphi^2 ds\right)^{1/2} R^j\sqrt{2\pi R} + \left(\int_\Gamma f^2 ds\right)^{1/2} jR^{j-1}\sqrt{2\pi R}\\
&\leq j\|\varphi\|_2 R^j\sqrt{2\pi R} + j\|f\|_2 R^{j-1}\sqrt{2\pi R}.
\end{aligned}$$

$$\begin{aligned}
|\beta_j| &= \left|\frac{R(v_j)}{-j}\right|\\
&\leq \|\varphi\|_2 R^j\sqrt{2\pi R} + \|f\|_2 R^{j-1}\sqrt{2\pi R}\\
&\leq \|\varphi\|_2 R^{2m}\sqrt{2\pi R} + \|f\|_2 R^{2m}\sqrt{2\pi R}
\end{aligned}$$

where $R > 1$.

Let

$$T = Z_2 Z_1^{-1} = Z_2\frac{\mathrm{adj}(Z_1)}{\det(Z_1)}$$

where $Z_1 = \begin{bmatrix} \beta_1 & \beta_2 & \cdots & \beta_m \\ \beta_2 & \beta_3 & \cdots & \beta_{m+1} \\ \vdots & & & \\ \beta_m & \beta_{m+1} & \cdots & \beta_{2m-1} \end{bmatrix}$ and $Z_2 = \begin{bmatrix} \beta_2 & \beta_3 & \cdots & \beta_{m+1} \\ \beta_3 & \beta_4 & \cdots & \beta_{m+2} \\ \vdots & & & \\ \beta_{m+1} & \beta_{m+2} & \cdots & \beta_{2m} \end{bmatrix}$.

We can view $R(v_j)$ as the measurement obtained by the "detector" v_j, while β_j is just a constant multiple of $R(v_j)$. So, β_j is still a measurement of another form, which contains the information about the moment and the position of the dipole source. Since Z_1 and Z_2 are constructed by different measurements β_j, T is also a matrix of measurements.

Assume T is the measurements without noise, and $\tilde{T}$ is the measurements with noise. Then,

$$\begin{aligned}
\|T - \tilde{T}\|_\infty &= \|Z_2 Z_1^{-1} - \tilde{Z}_2\tilde{Z}_1^{-1}\|_\infty\\
&\leq \|Z_2 - \tilde{Z}_2\|_\infty\|Z_1^{-1}\|_\infty + \|Z_1^{-1} - \tilde{Z}_1^{-1}\|_\infty\|Z_2\|_\infty.
\end{aligned}$$

We will analyse the four norms in the above inequality one by one.

$$\|Z_2 - \tilde{Z}_2\|_\infty \leq m\|\varphi - \tilde{\varphi}\|_2 R^{2m}\sqrt{2\pi R} + m\|f - \tilde{f}\|_2 R^{2m}\sqrt{2\pi R}.$$

To find $\|Z_1^{-1}\|_\infty$ we need to estimate $\|\mathrm{adj}(Z_1)\|_\infty$. We first observe the results for $m = 3$, then prove the results to the arbitrary m using mathematical induction.

If $Z_1 = \begin{bmatrix} \beta_1 & \beta_2 & \beta_3 \\ \beta_2 & \beta_3 & \beta_4 \\ \beta_3 & \beta_4 & \beta_5 \end{bmatrix}$, then the absolute value of the first element of $\mathrm{adj}(Z_1)$ would be

$$\mathrm{abs}\left(\begin{vmatrix} \beta_3 & \beta_4 \\ \beta_4 & \beta_5 \end{vmatrix}\right)$$

$$
\begin{aligned}
&= |\beta_3\beta_5 - \beta_4^2| \le |\beta_3| \cdot |\beta_5| + |\beta_4^2| \\
&= (p_1 S_1^2 + p_2 S_2^2 + p_3 S_3^2)(p_1 S_1^4 + p_2 S_2^4 + p_3 S_3^4) + (p_1 S_1^3 + p_2 S_2^3 + p_3 S_3^3)^2 \\
&\le (3p_{max}R^2)(3p_{max}R^4) + (3p_{max}R^3)^2 = 2(3p_{max}R^3)^2 \\
&= (3-1)!3^{3-1} p_{max}^{3-1} R^{3(3-1)} \\
&=: \max\left(\mathrm{abs}\left(\begin{vmatrix} \beta_3 & \beta_4 \\ \beta_4 & \beta_5 \end{vmatrix}\right)\right).
\end{aligned}
$$

Then,

$$
\begin{aligned}
&\| \mathrm{adj}(Z_1) \|_\infty \\
\le\ & \max\left(\mathrm{abs}\left(\begin{vmatrix} \beta_3 & \beta_4 \\ \beta_4 & \beta_5 \end{vmatrix}\right)\right) + \max\left(\mathrm{abs}\left(\begin{vmatrix} \beta_2 & \beta_4 \\ \beta_3 & \beta_5 \end{vmatrix}\right)\right) + \max\left(\mathrm{abs}\left(\begin{vmatrix} \beta_2 & \beta_3 \\ \beta_3 & \beta_4 \end{vmatrix}\right)\right) \\
\le\ & 3 \cdot \max\left(\mathrm{abs}\left(\begin{vmatrix} \beta_3 & \beta_4 \\ \beta_4 & \beta_5 \end{vmatrix}\right)\right) \\
=\ & 3 \cdot (3-1)!3^{3-1} p_{max}^{3-1} R^{3(3-1)} \\
=\ & 3!3^{3-1} p_{max}^{3-1} R^{3(3-1)}.
\end{aligned}
$$

Assume when $m = n - 1$, we have

$$
\mathrm{abs}\left(\begin{vmatrix} \beta_3 & \beta_4 & \cdots & \beta_{n+1} \\ \beta_4 & \beta_5 & \cdots & \beta_{n+2} \\ \vdots & & & \\ \beta_{n+1} & \beta_{n+2} & \cdots & \beta_{2n-1} \end{vmatrix}\right) \le (n-1)! n^{n-1} p_{max}^{n-1} R^{n(n-1)}.
$$

In fact, this inequality is also true for other minors with matrix size $(n-1) \times (n-1)$.

Then, when $m = n$ we have

$$
\begin{aligned}
&\mathrm{abs}\left(\begin{vmatrix} \beta_3 & \beta_4 & \cdots & \beta_{n+1} & \beta_{n+2} \\ \beta_4 & \beta_5 & \cdots & \beta_{n+2} & \beta_{n+3} \\ \vdots & & & & \\ \beta_{n+1} & \beta_{n+2} & \cdots & \beta_{2n-1} & \beta_{2n} \\ \beta_{n+2} & \beta_{n+3} & \cdots & \beta_{2n} & \beta_{2n+1} \end{vmatrix}\right) \\
\le\ & \max|\beta_{2n+1}| \cdot \max\left(\mathrm{abs}\left(\begin{vmatrix} \beta_3 & \beta_4 & \cdots & \beta_{n+1} \\ \beta_4 & \beta_5 & \cdots & \beta_{n+2} \\ \vdots & & & \\ \beta_{n+1} & \beta_{n+2} & \cdots & \beta_{2n-1} \end{vmatrix}\right)\right) + \cdots \\
&+ \max|\beta_{n+2}| \cdot \max\left(\mathrm{abs}\left(\begin{vmatrix} \beta_4 & \beta_5 & \cdots & \beta_{n+2} \\ \beta_5 & \beta_6 & \cdots & \beta_{n+3} \\ \vdots & & & \\ \beta_{n+2} & \beta_{n+3} & \cdots & \beta_{2n} \end{vmatrix}\right)\right)
\end{aligned}
$$

$$
\begin{aligned}
&\leq n \cdot \max|\beta_{2n+1}| \cdot \max\left\{\operatorname{abs}\left(\begin{vmatrix} \beta_3 & \beta_4 & \cdots & \beta_{n+1} \\ \beta_4 & \beta_5 & \cdots & \beta_{n+2} \\ \vdots & & & \\ \beta_{n+1} & \beta_{n+2} & \cdots & \beta_{2n-1} \end{vmatrix}\right)\right\} \\
&\leq n \cdot \max|p_1 S_1^{2n} + p_2 S_2^{2n} + \cdots + p_n S_n^{2n}| \cdot (n-1)! n^{n-1} p_{max}^{n-1} R^{n(n-1)} \\
&\leq n \cdot n p_{max} R^{2n} \cdot (n-1)! n^{n-1} p_{max}^{n-1} R^{n^2-n)} \\
&= n! n^n p_{max}^n R^{(n+1)n} \\
&\leq n!(n+1)^n p_{max}^n R^{(n+1)n}.
\end{aligned}
$$

Then, for any m we have

$$
\begin{aligned}
\|\operatorname{adj}(Z_1)\|_\infty &= \left\| \operatorname{adj}\left(\begin{bmatrix} \beta_1 & \beta_2 & \cdots & \beta_{m-1} & \beta_m \\ \beta_2 & \beta_3 & \cdots & \beta_m & \beta_{m+1} \\ \vdots & & & & \\ \beta_{m-1} & \beta_m & \cdots & \beta_{2m-3} & \beta_{2m-2} \\ \beta_m & \beta_{m+1} & \cdots & \beta_{2m-2} & \beta_{2m-1} \end{bmatrix}\right)\right\|_\infty \\
&\leq \max\left\{\operatorname{abs}\left(\begin{vmatrix} \beta_3 & \beta_4 & \cdots & \beta_{m+1} \\ \beta_4 & \beta_5 & \cdots & \beta_{m+2} \\ \vdots & & & \\ \beta_{m+1} & \beta_{m+2} & \cdots & \beta_{2m-1} \end{vmatrix}\right)\right\} + \cdots \\
&\quad + \max\left\{\operatorname{abs}\left(\begin{vmatrix} \beta_2 & \beta_3 & \cdots & \beta_m \\ \beta_3 & \beta_4 & \cdots & \beta_{m+1} \\ \vdots & & & \\ \beta_m & \beta_{m+1} & \cdots & \beta_{2m-2} \end{vmatrix}\right)\right\} \\
&\leq m \cdot \max\left\{\operatorname{abs}\left(\begin{vmatrix} \beta_3 & \beta_4 & \cdots & \beta_{m+1} \\ \beta_4 & \beta_5 & \cdots & \beta_{m+2} \\ \vdots & & & \\ \beta_{m+1} & \beta_{m+2} & \cdots & \beta_{2m-1} \end{vmatrix}\right)\right\} \\
&= m \cdot (m-1)! m^{m-1} p_{max}^{m-1} R^{m(m-1)} \\
&= m! m^{m-1} p_{max}^{m-1} R^{m(m-1)}.
\end{aligned}
$$

Thus,

$$
\begin{aligned}
\|Z_1^{-1}\|_\infty &= \left\| \frac{\operatorname{adj}(Z_1)}{\det(Z_1)} \right\|_\infty \\
&\leq \frac{m! m^{m-1} p_{max}^{m-1} R^{m(m-1)}}{p_1 p_2 \cdots p_m \prod_{1 \leq i < j \leq m} (S_i - S_j)^2} \\
&\leq \frac{m! m^{m-1} p_{max}^{m-1} R^{m(m-1)}}{p_{min}^m d^{m(m-1)}}
\end{aligned}
$$

where d is the smallest distance between any two dipoles.

Notice that

$$Z_1(Z_1^{-1} - \tilde{Z}_1^{-1}) + (Z_1 - \tilde{Z}_1)\tilde{Z}_1^{-1} = 0.$$

$$Z_1^{-1} - \tilde{Z}_1^{-1} = -Z_1^{-1}(Z_1 - \tilde{Z}_1)\tilde{Z}_1^{-1}.$$

$$\begin{aligned} & \|Z_1^{-1} - \tilde{Z}_1^{-1}\|_\infty \\ \leq\ & \|Z_1^{-1}\|_\infty \cdot \|Z_1 - \tilde{Z}_1\|_\infty \cdot \|\tilde{Z}_1^{-1}\|_\infty \\ \leq\ & \left(\frac{m!m^{m-1}p_{max}^{m-1}R^{m(m-1)}}{p_{min}^m d^{m(m-1)}}\right)^2 \cdot \left(m\|\varphi - \tilde{\varphi}\|_2 R^{2m}\sqrt{2\pi R} + m\|f - \tilde{f}\|_2 R^{2m}\sqrt{2\pi R}\right). \end{aligned}$$

Based on the above results, we have

$$\begin{aligned} & \|T - \tilde{T}\|_\infty \\ \leq\ & \|Z_2 - \tilde{Z}_2\|_\infty \|Z_1^{-1}\|_\infty + \|Z_1^{-1} - \tilde{Z}_1^{-1}\|_\infty \|Z_2\|_\infty \\ \leq\ & \left(m\|\varphi - \tilde{\varphi}\|_2 R^{2m}\sqrt{2\pi R} + m\|f - \tilde{f}\|_2 R^{2m}\sqrt{2\pi R}\right)\left(\frac{m!m^{m-1}p_{max}^{m-1}R^{m(m-1)}}{p_{min}^m d^{m(m-1)}}\right) \\ & + \left(\frac{m!m^{m-1}p_{max}^{m-1}R^{m(m-1)}}{p_{min}^m d^{m(m-1)}}\right)^2 \cdot \left(m\|\varphi\|_2 R^{2m}\sqrt{2\pi R} + m\|f\|_2 R^{2m}\sqrt{2\pi R}\right) \\ & \cdot \left(m\|\varphi - \tilde{\varphi}\|_2 R^{2m}\sqrt{2\pi R} + m\|f - \tilde{f}\|_2 R^{2m}\sqrt{2\pi R}\right) \\ \leq\ & 2m\left(\|\varphi\|_2 R^{2m}\sqrt{2\pi R} + \|f\|_2 R^{2m}\sqrt{2\pi R}\right)\left(\frac{m!m^{m-1}p_{max}^{m-1}R^{m(m-1)}}{p_{min}^m d^{m(m-1)}}\right) \\ & + 2m^2\left(\|\varphi\|_2 R^{2m}\sqrt{2\pi R} + \|f\|_2 R^{2m}\sqrt{2\pi R}\right)^2\left(\frac{m!m^{m-1}p_{max}^{m-1}R^{m(m-1)}}{p_{min}^m d^{m(m-1)}}\right)^2. \end{aligned} \tag{3.3}$$

We can further simplify it as

$$\|T - \tilde{T}\|_\infty \leq E + E^2 \tag{3.4}$$

where

$$E = 2mR^{2m}\sqrt{2\pi R}\,(\|f\|_2 + \|\varphi\|_2)\left(\frac{m!m^{m-1}p_{max}^{m-1}R^{m(m-1)}}{p_{min}^m d^{m(m-1)}}\right). \tag{3.5}$$

When $0 < E < 1$, the error in the position estimate is mainly controlled by E; when $E > 1$, the error in the position estimate is mainly controlled by E^2. □

4. Numerical simulation results

4.1. Numerical simulation for 2D

Let Ω be a circular disk centered at the origin and of radius $r = 1$. Then, the numerical implementation can be simplified as follow.

$$\frac{\partial v_j}{\partial v} = \frac{\partial(x+iy)^j}{\partial r} = \frac{\partial\left(re^{i\theta}\right)^j}{\partial r} = jr^{j-1}e^{i\theta j} = \frac{jr^j e^{i\theta j}}{r} = \frac{jv_j}{r}.$$

$$\begin{aligned} R(v_j) &= -\left\langle f, \frac{\partial v_j}{\partial \nu} \right\rangle \\ &= -\int_\Gamma f \cdot \frac{\partial v_j}{\partial \nu} d\Gamma \\ &= -\int_0^{2\pi} f \cdot \frac{j v_j}{r} \cdot r d\theta \\ &= -j \int_0^{2\pi} f \cdot v_j d\theta \\ &= -j \int_0^{2\pi} f \cdot \left(re^{i\theta}\right)^j d\theta, \end{aligned}$$

where f is a function of θ on the boundary. We do not need to know the explicit form of f, but we can measure as many points as possible on the boundary to get enough discretized function values of f. Then, the above integral can be approximated by a Riemann sum.

The measurable values we want to use in the following are

$$\beta_j = -\frac{R(v_j)}{j} = \int_0^{2\pi} f \cdot \left(re^{i\theta}\right)^j d\theta.$$

The Romberg algorithm is used to calculate the integral numerically.

We compare the efficacy of the harmonic function method in dipolar source reconstruction when the perturbation level is $0, 0.001, 0.01, 0.1$ and the number of dipoles is $1, 2, 3, 4, 5$. It is shown that as the perturbation level increases, the reconstruction error increases (see Figures 1–5).

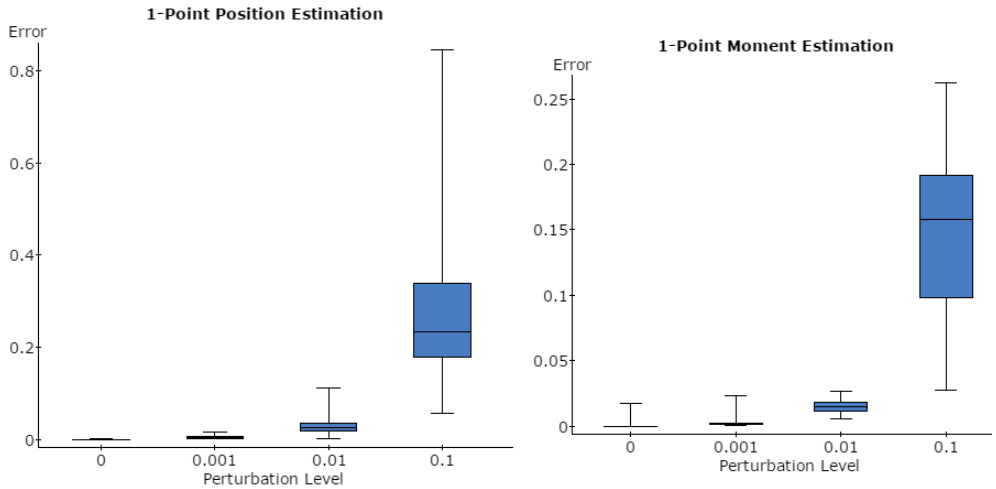

Figure 1. The effect of the perturbation level on the reconstruction error of 1 dipole. As the perturbation level increases, the reconstruction error increases. Here, the perturbation means adding noise to the exact measurement. If the perturbation level is σ, then the perturbed measurement is the exact measurement times $(1 \pm \sigma)$, where plus or minus signs are randomly assigned to each channel. Also, the error is defined as the sum of position errors.

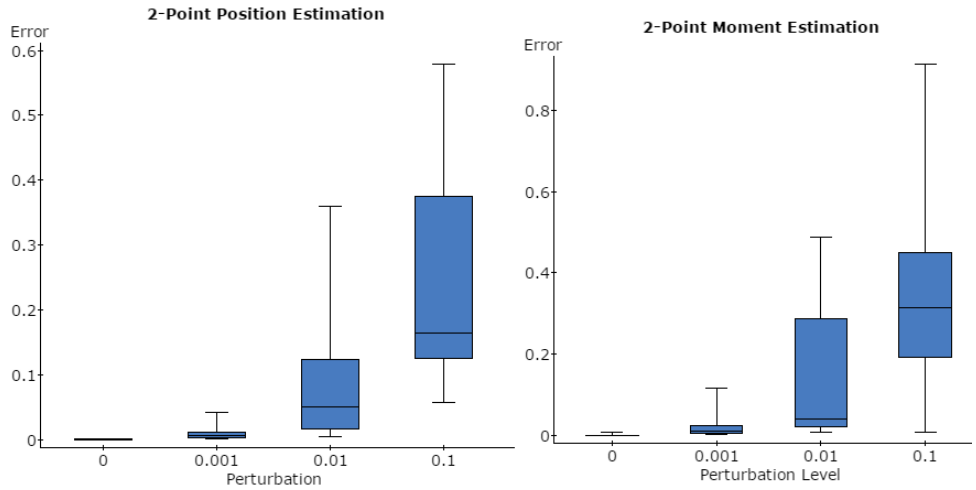

Figure 2. The effect of the perturbation level on the reconstruction error of 2 dipoles. As the perturbation level increases, the reconstruction error increases. Here, the perturbation means adding noise to the exact measurement. If the perturbation level is σ, then the perturbed measurement is the exact measurement times $(1 \pm \sigma)$, where plus or minus signs are randomly assigned to each channel. Also, the error is defined as the sum of position errors.

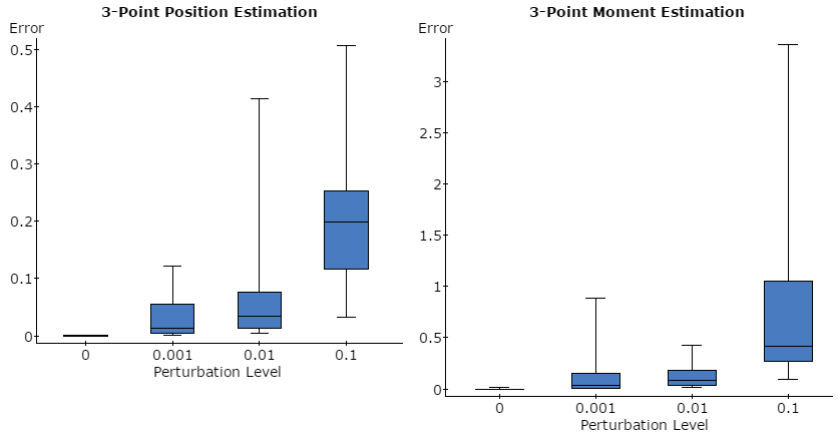

Figure 3. The effect of the perturbation level on the reconstruction error of 3 dipoles. As the perturbation level increases, the reconstruction error increases. Here, the perturbation means adding noise to the exact measurement. If the perturbation level is σ, then the perturbed measurement is the exact measurement times $(1 \pm \sigma)$, where plus or minus signs are randomly assigned to each channel. Also, the error is defined as the sum of position errors.

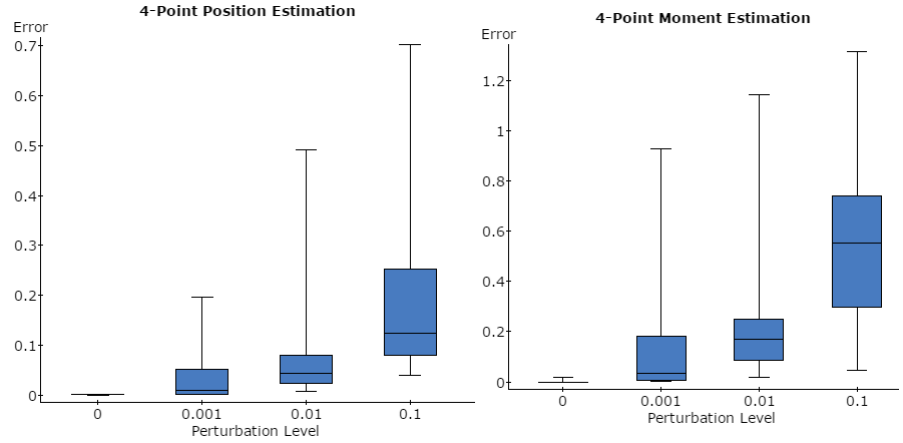

Figure 4. The effect of the perturbation level on the reconstruction error of 4 dipoles. As the perturbation level increases, the reconstruction error increases. Here, the perturbation means adding noise to the exact measurement. If the perturbation level is σ, then the perturbed measurement is the exact measurement times $(1 \pm \sigma)$, where plus or minus signs are randomly assigned to each channel. Also, the error is defined as the sum of position errors.

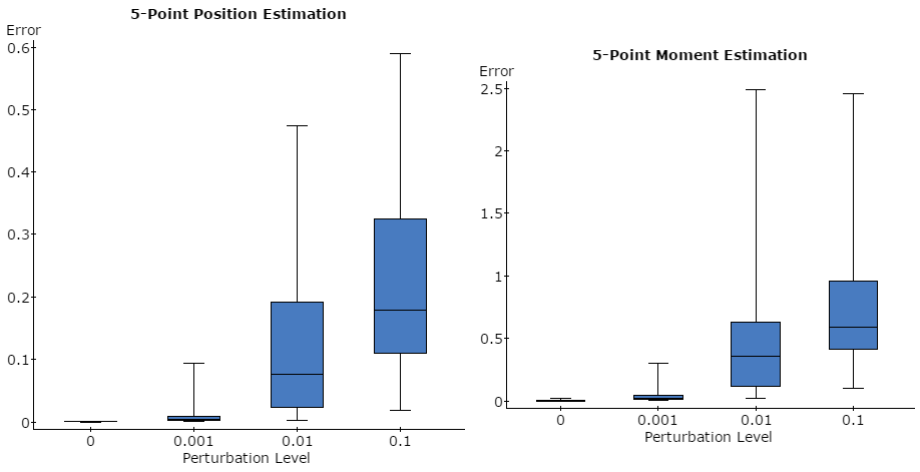

Figure 5. The effect of the perturbation level on the reconstruction error of 5 dipoles. As the perturbation level increases, the reconstruction error increases. Here, the perturbation means adding noise to the exact measurement. If the perturbation level is σ, then the perturbed measurement is the exact measurement times $(1 \pm \sigma)$, where plus or minus signs are randomly assigned to each channel. Also, the error is defined as the sum of position errors.

In the following we show the results of source estimation, assuming there are 3 dipolar sources ($m = 3$).

- Dipole 1: position $(0.3, -0.3)$ and moment $(0, 1)$.
- Dipole 2: position $(0.6, 0.2)$ and moment $(1, 1)$.
- Dipole 3: position $(-0.5, 0.4)$ and moment $(2, 2)$.

In the graphs (see Figure 6) we use a small circle and a red line segment to indicate the true value, and use a cross sign and a green line segment to indicate the reconstructed values.

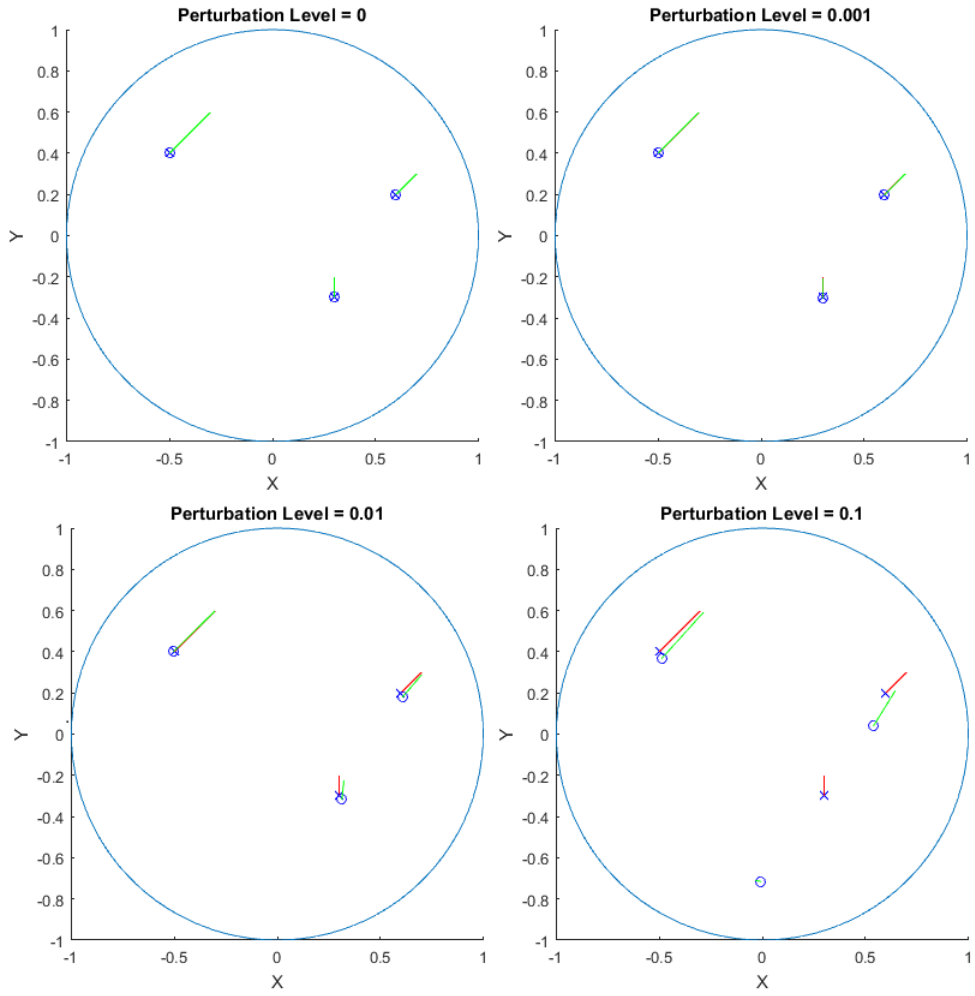

Figure 6. The effect of the perturbation level on the reconstruction error of 3 dipoles. As the perturbation level increases, the reconstruction error increases

From error estimates we know that as the distance between two dipoles gets closer, the reconstruction error for the positions of dipoles gets larger (see Table 1 and Figure 7). This is verified by the numerical simulations.

We randomly assign two dipoles with fixed distance, say 0.1, in the unit disk, then reconstruct their positions. We fix the noise level for all experiments at $\sigma = 0.001$.

Table 1. The effect of dipole distance on the reconstruction error. As two dipoles get closer, the mean reconstruction error in the positions of the dipoles gets larger, which is consistent with the result in the error estimate.

Exact Dipole Distance	Reconstructed Dipole Distance
0.03	0.7429
0.05	0.3084
0.10	0.1200

Let d_i $(i = 1, 2)$ be the distance between the ith exact dipole and the ith estimated dipole, and d_{max} be the largest d.

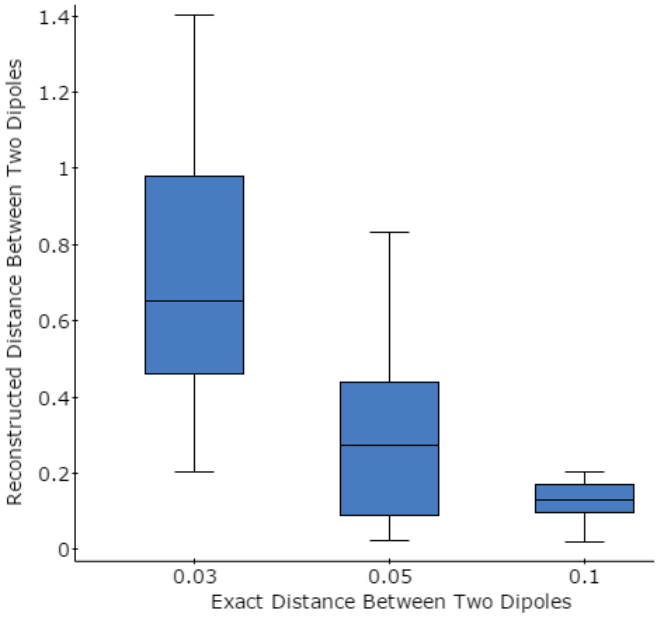

Figure 7. The effect of dipole distance on the reconstruction error. As two dipoles get closer, the reconstruction error in the positions of the dipoles gets larger, which is consistent with the theoretical analysis in the error estimate. When $d_{exact} = 0.10$, $\overline{d_{est}} = 0.1200$; when $d_{exact} = 0.05$, $\overline{d_{est}} = 0.3084$; when $d_{exact} = 0.03$, $\overline{d_{est}} = 0.7429$

We repeat the experiment 10 times and show their performance on average over different dipole distances.

The above experiment also provides a numerical example to show that the estimate given by us in Theorem 3.1 provides a better error bound when the two poles are very close.

When the number of dipoles is $m = 2$, Chafik's estimate is bounded by $\dfrac{C_1}{d}$ (see Inequality (3.1)), while our estimate is bounded by $\dfrac{C_2}{d^2}$ (see Inequality (3.4) and Eq (3.5)) where d is the smallest distance between two dipoles and C_i $(i = 1, 2)$ are constants independent of d. That is, when the distance is halved, the error bound will be amplified by 2 in Chafik's estimate and by 4 in our estimate.

From the data simulation, we see that

$$\frac{0.05}{0.03} = 1.67 < \frac{0.7429}{0.3084} = 2.41 < 1.67^2 = 2.79.$$

$$\frac{0.10}{0.05} = 2 < \frac{0.3084}{0.1200} = 2.57 < 2^2 = 4.$$

$$\frac{0.10}{0.03} = 3.33 < \frac{0.7429}{0.1200} = 6.19 < 3.33^2 = 11.09.$$

For example, when the distance between the two dipoles is reduced from 0.10 to 0.05, by Chafik's estimate the error should be amplified by 2, but in fact, the error is amplified by 2.57, which is bounded by 4 in our estimate.

5. Conclusions

In this paper we studied a harmonic function method for the dipolar source reconstruction, derived error estimate for the harmonic function method and compared our result with Chafik's estimate. By numerical simulations it is shown that the harmonic function method can quickly and accurately locate active regions in EEG source reconstruction. In the future, we plan to extend the harmonic function method to 3D case and applied this method to some real EEG data. The brain's conductance variation in different brain regions also leads to additional challenges in source localization [35]. Although these tissue properties can be quantified through MRI methods, numerical methods such as finite element method will be needed to solve the inverse problems. Since the estimation of the number of dipoles relies on the calculation of the rank of the measurement matrix, which is significantly affected by the noise, we hope to find some way to solve or circumvent this problem. In addition, the situation that the number of exact dipoles is not equal to the estimated value could also be considered. Furthermore, when two dipoles get close enough, it may be better to regard them as an equivalent dipole to avoid increased error.

Acknowledgments

We thank anonymous reviewers for providing us with valuable suggestions.

Conflict of interest

All authors declare no conflicts of interest in this paper.

References

1. N. K. Logothetis, What we can do and what we cannot do with fMRI, *Nature*, **453** (2008), 869–878. https://doi.org/10.1038/nature06976
2. B. He, J. Lian, High-resolution spatio-temporal functional neuroimaging of brain activity, *Crit. Rev. Biomed. Eng.*, **30** (2002), 283–306. https://doi.org/10.1615/CritRevBiomedEng.v30.i456.30

3. P. L. Nunez, *Electric Fields of the Brain: The Neurophysics of EEG*, Oxford University Press, 1981.
4. R. Grave de Peralta Menendez, S. L. Gonzalez Andino, S. Morand, C. M. Michel, T. Landis, Imaging the electrical activity of the brain: ELECTRA, *Hum. Brain Mapp.*, **9** (2000), 1–12. https://doi.org/10.1002/(SICI)10970193(2000)9:1<1::AIDHBM1>3.0.CO;2#
5. C. M. Michel, M. M. Murray, G. Lantz, S. Gonzalez, L. Spinelli, R. Grave de Peralta, EEG source imaging, *Clin. Neurophysiol.*, **115** (2004), 2195–2222. https://doi.org/10.1016/j.clinph.2004.06.001
6. A. Hunter, B. Crouch, N. Webster, B. Platt, Delirium screening in the intensive care unit using emerging qeeg techniques: A pilot study, *AIMS Neurosci.*, **7** (2020), 1–16. https://doi.org/10.3934/Neuroscience.2020001
7. G. V. Portnova, O. Ivanova, E. V. Proskurnina, Effects of eeg examination and aba-therapy on resting-state eeg in children with low-functioning autism, *AIMS Neurosci.*, **7** (2020), 153–167. https://doi.org/10.3934/Neuroscience.2020011
8. R. Grech, T. Cassar, J. Muscat, K. P. Camilleri, S. G. Fabri, M. Zervakis, et al., Review on solving the inverse problem in EEG source analysis, *J. NeuroEng. Rehabilitation*, **5** (2008), 25. https://doi.org/10.1186/1743-0003-5-25
9. V. Isakov, *Inverse Problems for Partial Differential Equations*, Springer, 2nd edition, 2005.
10. S. Vessella, Locations and strengths of point sources: stability estimates, *Inverse Probl.*, **8** (1992), 911. https://doi.org/10.1088/0266-5611/8/6/008
11. R. M. Leahy, J. C. Mosher, M. E. Spencer, M. X. Huang, J. D. Lewine, A study of dipole localization accuracy for meg and eeg using a human skull phantom, *Electroencephalogr. clin. neurophysiol.*, **107** (1998), 159–173. https://doi.org/10.1016/S0013-4694(98)00057-1
12. A. El Badia, T. Ha-Duong, An inverse source problem in potential analysis, *Inverse Probl.*, **16** (2000), 651–663. https://doi.org/10.1088/0266-5611/16/3/308
13. M. Chafik, A. El Badia, T. Ha-Duong, On some inverse eeg problems, *Inverse Probl. Eng. Mech. II*, pages 537–544, 2000. https://doi.org/10.1016/B978-008043693-7/50129-X
14. T. Nara, S. Ando, A projective method for an inverse source problem of the poisson equation, *Inverse Probl.*, **19** (2003), 355–369. https://doi.org/10.1088/0266-5611/19/2/307
15. H. Kang, H. Lee, Identification of simple poles via boundary measurements and an application of eit, *Inverse Probl.*, **20** (2004), 1853. https://doi.org/10.1088/0266-5611/20/6/010
16. A. El Badia, Inverse source problem in an anisotropic medium by boundary measurements, *Inverse Probl.*, **21** (2005), 1487. https://doi.org/10.1088/0266-5611/21/5/001
17. L. Baratchart, A. Ben Abda, F. Ben Hassen, J. Leblond, Recovery of pointwise sources or small inclusions in 2d domains and rational approximation, *Inverse Probl.*, **21** (2005), 51. https://doi.org/10.1088/0266-5611/21/1/005
18. Y. S. Chung, S. Y. Chung, Identification of the combination of monopolar and dipolar sources for elliptic equations, *Inverse Probl.*, **25** (2009), 085006. https://doi.org/10.1088/0266-5611/25/8/085006

19. D. Kandaswamy, T. Blu, D. van de Ville, Analytic sensing: Noniterative retrieval of point sources from boundary measurements, *SIAM J. Sci. Comput.*, **31** (2009), 3179–3194. https://doi.org/10.1137/080712829

20. T. Nara, S. Ando, Direct localization of poles of a meromorphic function from measurements on an incomplete boundary, *Inverse Probl.*, **26** (2010), 015011. https://doi.org/10.1088/0266-5611/26/1/015011

21. A. El Badia, T. Nara, An inverse source problem for helmholtz's equation from the cauchy data with a single wave number, *Inverse Probl.*, **27** (2011), 105001. https://doi.org/10.1088/0266-5611/27/10/105001

22. M. Clerc, J. Leblond, J.-P. Marmorat, T. Papadopoulo, Source localization using rational approximation on plane sections, *Inverse Probl.*, **28** (2012), 055018. https://doi.org/10.1088/0266-5611/28/5/055018

23. R. Mdimagh, I. Ben Saad, Stability estimates for point sources identification problem using reciprocity gap concept via the helmholtz equation, *Appl. Math. Model.*, **40** (2016), 7844–7861. https://doi.org/10.1016/j.apm.2016.03.024

24. J. Vorwerk, Ü. Aydin, C. H. Wolters, C. R. Butson, Influence of head tissue conductivity uncertainties on eeg dipole reconstruction, *Front Neurosci.*, **13** (2019), PMCID: PMC6558618. https://doi.org/10.3389/fnins.2019.00531

25. M. Rubega, M. Carboni, M. Seeber, D. Pascucci, S. Tourbier, G. Toscano, et al., Estimating eeg source dipole orientation based on singular-value decomposition for connectivity analysis, *Brain topogr.*, **32** (2019), 704–719. https://doi.org/10.1007/s10548-018-0691-2

26. M. S. Hämäläinen, R. J. Ilmoniemi, Interpreting magnetic fields of the brain: minimum norm estimates, *Med. Biol. Eng. & Comput.*, **32** (1994), 35–42. https://doi.org/10.1007/BF02512476

27. R. D. Pascual-Marqui, Review of methods for solving the eeg inverse problem, *Int. J. Bioelectromagn.*, **1** (1999), 75–86, 1999.

28. S. Baillet, Toward functional brain imaging of cortical electrophysiology markovian models for magneto and electroencephalogram source estimation and experimental assessments, *Orsay, France*, 1998.

29. S. Baillet, J. C. Mosher, R. M. Leahy, Electromagnetic brain mapping, *IEEE Signal Process. Mag.*, **18** (2001), 14–30. https://doi.org/10.1109/79.962275

30. J. C. Mosher, P. S. Lewis, R. M. Leahy, Multiple dipole modeling and localization from spatio-temporal MEG data, *IEEE Trans. Biomed. Eng.*, **39** (1992), 541–557. https://doi.org/10.1109/10.141192

31. P. A. Muñoz Gutiérrez, E. Giraldo, M. Bueno-López, M. Molinas, Localization of active brain sources from eeg signals using empirical mode decomposition: a comparative study, *Front. Integrat. Neurosci.*, **2** (2018), 55. https://doi.org/10.3389/fnint.2018.00055

32. C. Kaur, P. Singh, S. Sahni, Electroencephalography-based source localization for depression using standardized low resolution brain electromagnetic tomography-variational mode decomposition technique, *Eur. Neurol.*,**81** (2019), 63–75. https://doi.org/10.1159/000500414

33. V. P. Oikonomou, I. Kompatsiaris, A novel bayesian approach for eeg source localization, *Comput. Intell. Neurosci.*, 2020. https://doi.org/10.1155/2020/8837954

34. S. Andrieux, A. Ben Abda, H.D. Bui, Reciprocity principle and crack identification, *Inverse Probl.*, **15** (1999), 59. https://doi.org/10.1088/0266-5611/15/1/010

35. H. Azizollahi, M. Darbas, M. M. Diallo, A. El Badia, S. Lohrengel, EEG in neonates: Forward modeling and sensitivity analysis with respect to variations of the conductivity, *Math. Biosci. Eng.*, **15** (2018), 905–932. https://doi.org/10.3934/mbe.2018041

AIMS Press

© 2022 the Author(s), licensee AIMS Press. This is an open access article distributed under the terms of the Creative Commons Attribution License (http://creativecommons.org/licenses/by/4.0)